Electronic Supplementary Material (ESI) for Reaction Chemistry & Engineering.
This journal is © The Royal Society of Chemistry 2022

Supporting Information

On-the-Spot Quenching for Effective Implementation of Cooling Crystallization in Continuous-Flow Microfluidic Device

Paria Coliaie[1], Manish S. Kelkar[2], Marianne Langston[3], Chengxiang Liu[4], Daniel Patience[5], Dimitri Skliar[6], Nandkishor K. Nere[1,2], and Meenesh R. Singh[1,*]

Paria Coliaie[1], Manish S. Kelkar[2], Akshay Korde[2], Marianne Langston[3], Chengxiang Liu[4], Neda Nazemifard[5], Daniel Patience[4], Dimitri Skliar[6], Nandkishor K. Nere[1,2], and Meenesh R. Singh[1,*]

[1]Department of Chemical Engineering, University of Illinois at Chicago, Chicago, IL 60607
[2]Center of Excellence for Isolation & Separation Technologies (CoExIST), Process R&D, AbbVie Inc., North Chicago, IL 60064
[3]Pharmaceutics Research – Analytical Development, Takeda Pharmaceuticals International Co., Cambridge, MA 02139
[4]Pharmaceutical Development, Biogen, Cambridge, MA 02142
[5]Chemical Process Development, Takeda Pharmaceuticals International Co., Cambridge, MA 02139
[6]Chemical Process Development, Product Development, Bristol Myers Squibb Co., New Brunswick, NJ 08901

Corresponding Author:

Prof. Meenesh R. Singh
Assistant Professor
Department of Chemical Engineering
929 W. Taylor St.
University of Illinois at Chicago
Chicago, IL 60607
Tel: (312) 996-3424
Email: mrsingh@uic.edu

Keywords: Continuous Crystallization, Cooling Crystallization, Polymorph Screening, Growth Rates, Continuous-Flow Microfluidics

Table of Contents

S1. Comparative Analysis of Different Cooling Techniques

Different types of cooling techniques have been employed for microtiter and microfluidic systems. A comparative analysis of these four cooling techniques to effectively reduce the temperature of inlet solution with minimum gradients is provided in Table S1.

Table S1: Comparative Analysis of Different Cooling Techniques

	Thermoelectric Cooling	**Endothermic Cooling**	**Convective Cooling**	**Cooling Via Mixing**
Temperature Gradient along the microchannel	• Low with conductive material and low thickness • High with materials with low conductivity and high thickness	Medium	Low	• Low with Proper insulation • High without insulation
Supersaturation along the microchannel	Not Constant	Not Constant	Not Constant	Not Constant

The two selected strategies studied in this paper are labeled as follows throughout the manuscript.

Table S2: Labels for the on-spot-quenching strategies and the device used for each

Approach	**Device Label**	**Method**
First	Jacketed microfluidic mixer	Cooling jacket strategy
Second	Non-jacketed microfluidic mixer	Hot-and-cold-mixing strategy

S2. Jacketed Microfluidic Device: Design, Dimension, and Fabrication

S2.1 Justification of the Dimension Selection of the Microfluidic Device

The microfluidic mixer design is designed to enable homogenous mixing by enabling convective and diffusive mixing simultaneously. It includes a cylinder with four tangential inlet channels on the bottom plane and one outlet close to the top end. Every other inlet is merged into a single connection to decrease the number of the required pumps for the operation. The minimum size of the printable channels with the Form 2 3D printer is 1 mm, and the diameter of the cylinder is changed accordingly to allow for the placement of four tangential inlets. The connections are required to be equal to avoid pressure drops in the inlet connections. Therefore, the minimum length is selected for the merged connection in which they are equal.

S2.2 Dimensions

Figure S1, top, shows the isometric and top views of the jacketed microfluidic mixer with the marked dimensions. The required dimensions for drawing the merged-inlet single-well device are provided in Table S3. The non-jacketed microfluidic mixer has the exact dimensions for interior channels.

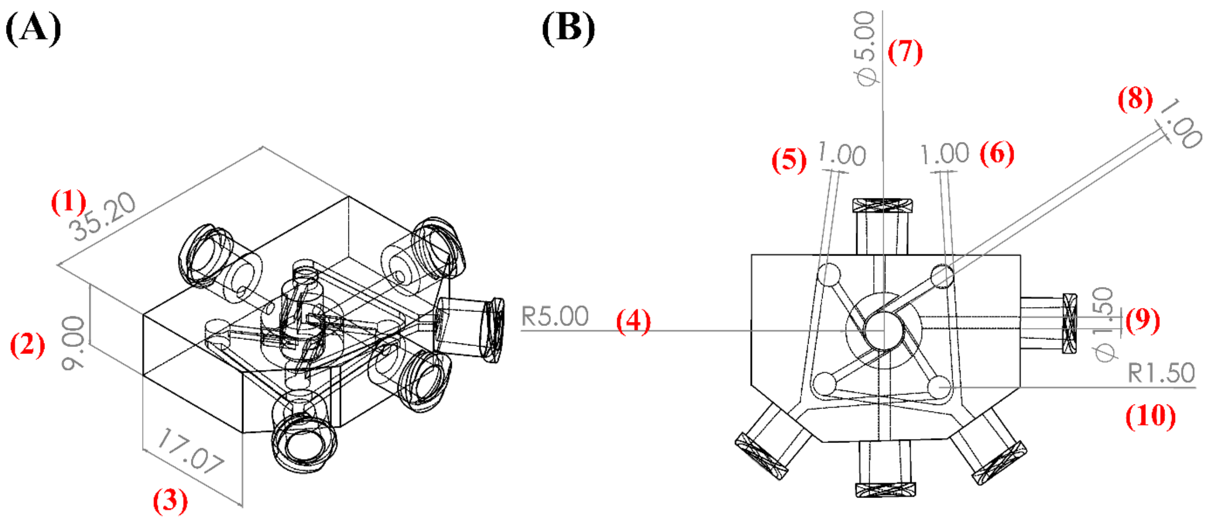

Figure S1: (A) Isometric view, **(B)** Top view of the jacketed microfluidic mixer device with dimensions marked.

Table S3: Dimensions of the jacketed microfluidic mixer device

Dimensions	Value (mm)
1	32.2
2	9
3	17.07
4	5
5	1
6	1
7	5
8	1
9	1.5
10	1.5

** The microfluidic mixer device used for mixing hot-and cold mixing strategy has identical dimensions to the jacketed microfluidic mixer, but the cooling bath and its inlet and outlet are eliminated.

S2.3 Fabrication

The microfluidic devices were fabricated using stereolithography (SLA) 3D printing technology. The CAD design of the microfluidic devices is prepared with SolidWorks® (2020, Dassault Systems), and then a commercial 3D printer (form 3, Formlabs Inc., USA) is used to print the microfluidic devices. The selected resin for the prints was the clear resin which is chemically resistant to various solvents, including ethanol and water. After printing the device, they are washed in an isopropyl alcohol (IPA) (90%, Sigma-Aldrich) bath for 20 mins in the Form Wash (Formlabs Inc., USA) to remove the residues of the resin from the external surface. The interior channels of the 3D printed device were washed separately by injecting IPA using a syringe to eliminate the uncured residues of the resin in the channels.

As shown in Figure 1A in the manuscript, the top and bottom faces of the microfluidic mixer were kept open to maximize optical clarity. The open holes on both sides were sealed with polycarbonate films using a fresh, clear resin. First, the area around the circular zone is covered with fresh uncured resin (from the resin tank), and a polycarbonate film is put on that. Next, the device is cured under UV light for 10 minutes to seal the open area.

S3. COMSOL Simulation of the Merged-Inlet Microfluidic Device

S3.1 Laminar Flow Module: Equations and Boundary Conditions

The laminar flow module of COMSOL was used to calculate the velocity profile in the microfluidic mixer. The time-dependent Navier Stock equation solved is described as follows:

$$\rho\frac{\partial u}{\partial t} + \rho(u.\nabla)u = \nabla.[-p.I + \mu(\nabla u + (\nabla u)^T) + F \qquad \textbf{Eq (1)}$$

Where ρ and μ are temperature-dependent density and the viscosity of water which is assumed to be incompressible.

Here the selected boundary conditions for the two temperature controlling strategies are listed:

- **Strategy 1: Cooling bath implementation:**

Figure S2A shows the isometric view of the imported 3D file of the jacketed microfluidic mixer device in the COMOSL Multiphysics for the simulation. In Figure S2B, the assigned boundary conditions for this system are shown and listed as:

Boundary Conditions:

→ Inlet $_{1,\text{Mixer}}$ = Inlet $_{2,\text{Mixer}}$ = Inlet $_{3,\text{Mixer}}$ = Inlet $_{4,\text{Mixer}}$: Q_{Mixer} = 0.25 mL.min^{-1}
→ Outlet $_{\text{Mixer}}$: $P = 1$ atm
→ Inlet $_{\text{Bath}}$: $Q_{Bath} = 10$ mL.min^{-1}
→ Outlet $_{\text{Bath}}$: $P = 1$ atm

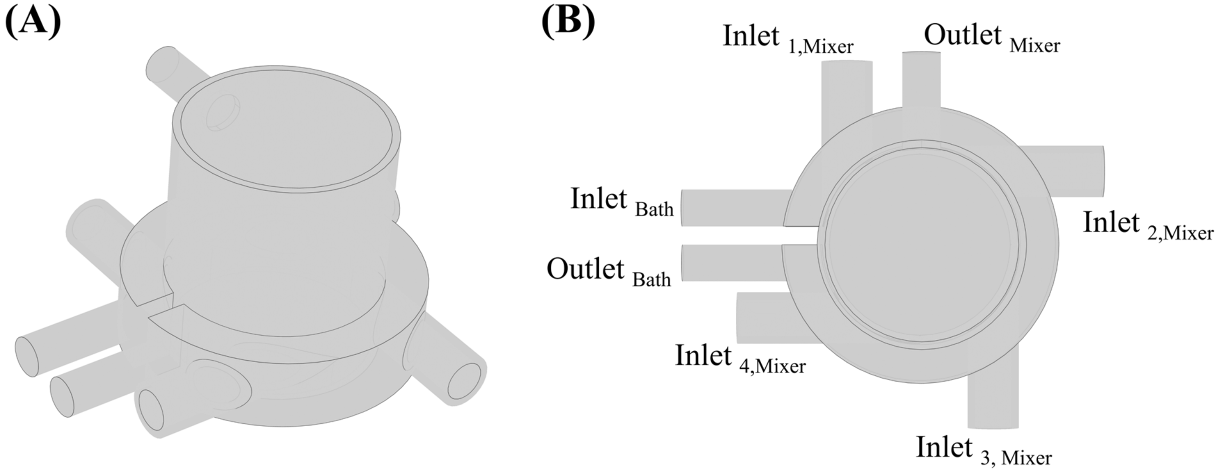

Figure S2: (A) Isometric view of the jacketed microfluidic device ;**(B)** The top view of the jacketed microfluidic device with the assigned boundary conditions for the mixer and cooling bath in the cooling bath strategy.

- **Strategy 2: Mixing saturated hot and cold streams:**

Figure S3A shows the isometric view of the imported 3D file of the microfluidic mixer device in COMOSL Multiphysics for the simulation. In Figure S3B, the assigned boundary conditions for this system are shown and listed as:

Boundary Conditions:

→ Inlet $_{1,\text{ Mixer}}$ = Inlet $_{3,\text{ Mixer}}$: $Q_{Hot} = 0.25$ mL.min^{-1}
→ Inlet $_{2,\text{ Mixer}}$ = Inlet $_{4,\text{ Mixer}}$: $Q_{Cold} = 0.25$ mL.min^{-1}
→ Outlet $_{\text{Mixer}}$: $P = 1$ atm

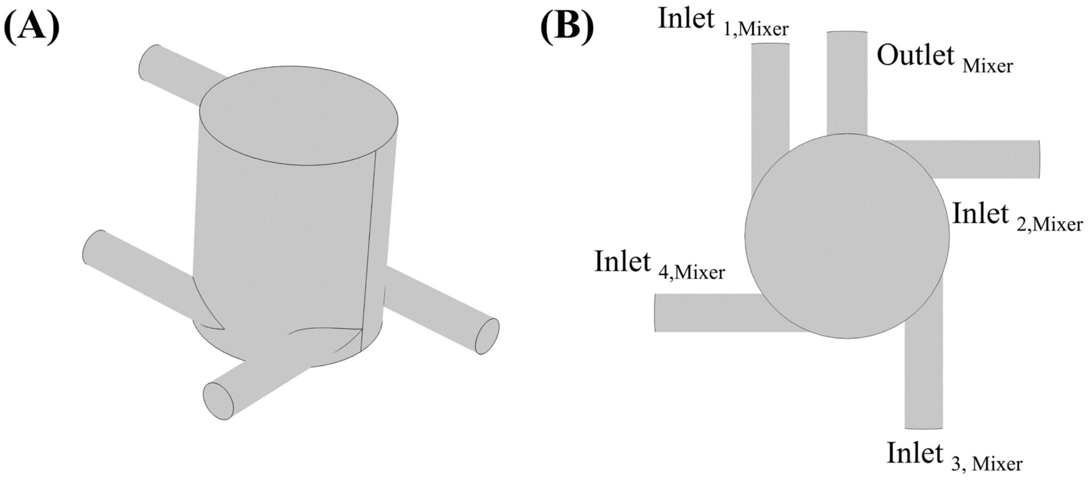

Figure S3: (A) Isometric view of the non-jacketed microfluidic mixer; **(B)** The top view of the non-jacketed microfluidic mixer with the assigned boundary conditions for the mixer in mixing hot and cold strategy.

The laminar flow module is coupled with the heat transfer in solid and fluid module modules, and all the assigned temperatures conditions are listed in section S2.2.

S3.2 Heat Transfer Module: Equations and Boundary Conditions

- **Strategy 1: Cooling bath implementation**

The heat transfer in the solids and fluids module is coupled with the laminar flow module to predict the equilibrium temperature profile in the microfluidic mixer device. The time-dependent energy balance equation is:

$$\rho c_P u.\nabla T + \nabla(-k\nabla T) = Q \qquad \textbf{Eq (2)}$$

Here, the bath walls are selected as the solid walls with PMMA selected as its material. The bath fluid and mixing fluids are also separated, and their boundary conditions, as shown in Figure 3A, are listed as:

→ Inlet $_{1,\text{ Mixer}}$ = Inlet $_{2,\text{ Mixer}}$ = Inlet $_{3,\text{ Mixer}}$ = Inlet $_{4,\text{ Mixer}}$: $T_{Hot} = 70\ ℃$
→ Outlet $_{\text{Mixer}}$: $-n.q = 0$
→ Inlet $_{\text{Bath}}$: $T_c = 20\ ℃$
→ Outlet $_{\text{Bath}}$: $-n.q = 0$

All other boundaries were set at the thermal insulation boundary.

- **Strategy 2: Mixing saturated hot and cold streams:**

The heat transfer in the fluids module is coupled with the laminar flow module to predict the equilibrium temperature profile in the microfluidic mixer device. The time-dependent energy balance equation is:

$$\rho c_P u.\nabla T + \nabla(-k\nabla T) = Q \qquad \textbf{Eq (3)}$$

where k is the thermal conductivity, ρ is the density and c_P is the heat capacity at constant pressure. In Figure S3B, boundaries with certain conditions are indicated and listed as:

Boundary Conditions:

→ Inlet 1, Mixer = Inlet 3, Mixer : $T_{Hot} = 70\ ℃$
→ Inlet 2, Mixer = Inlet 4, Mixer : $T_{Cold} = 20\ ℃$
→ Outlet Mixer: $-n.q = 0$

All other boundaries were set at the thermal insulation boundary.

S3.3 Model Parameters of the Simulations

In this study, we have simulated a coupled analysis of the laminar flow module and heat transfer in solids and fluids to evaluate the velocity, pressure, and temperature profile inside the microfluidic mixer and the cooling jacket. The 3D model for simulations was imported into the model from a Solid Work design. The design was further simplified by eliminating the sharp edges and smoothening the surfaces to enhance the mesh quality. The free tetrahedral mesh was selected for the models. The tetrahedral mesh was selected for this study, and the details are provided in the following part:

- Maximum Element Size = 1.15 mm
- Minimum Element Size = 0.207 mm
- Maximum Element Growth Rate = 1.5
- Curvature Factor = 0.6
- Resolution of Narrow Region = 0.5

The coupled equations of the Navier stock and mass balance were solved in the stationary solver using “PARDISO” solver. The residual tolerance was set to 0.01 with 100 iterations and left preconditioning. Newton was selected as the non-linear method with a damping factor of 0.1 and tolerance as the termination technique. The relative tolerance was also kept at 0.001. The temperature-dependent viscosity and density of the water were considered in the model.

S3.4 Temperature Homogeneity Index for Cooling Jackets with longer height

As mentioned in section 2.1 in the manuscript, one of the design considerations is to have a shorter height of cooling jacket not exceeding the diameter of the inlet. Here, we have shown the thermal homogeneity index for a cooling bath design with a longer height. Figure S4A shows the temperature profile of the mixer and the bath. Unlike the temperature profile shown in Figure 3A, the temperature decreases in the mixer as it goes toward the outlet. Figure S4B shows the thermal homogeneity index for the cooling bath design with a longer height. The index does not Plato as the distance from the bottom increases.

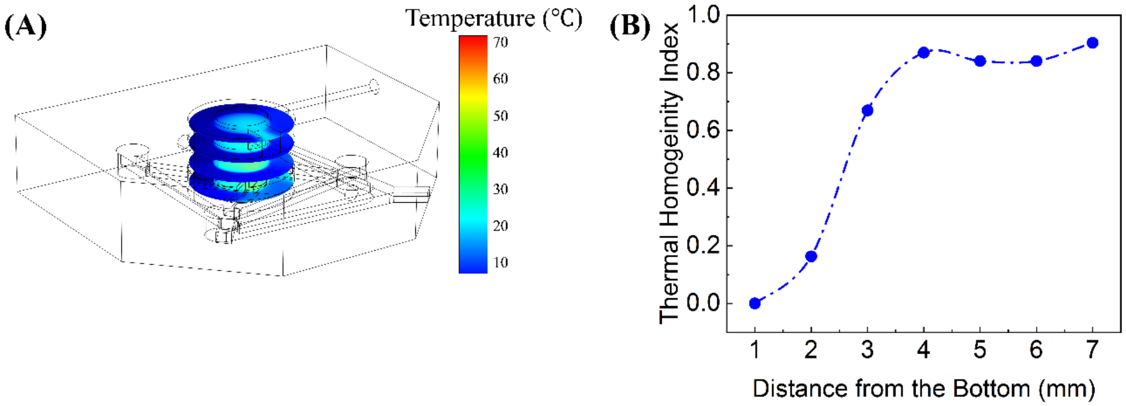

S3.5 Temperature Gradient Along the Radial Direction in the Microfluidic Mixer Device

Using the 3D temperature profile in each strategy, we extracted the temperature of a cut line in the radial direction at different mixer heights. The extracted data were plotted together in Figures S5A and S5B.

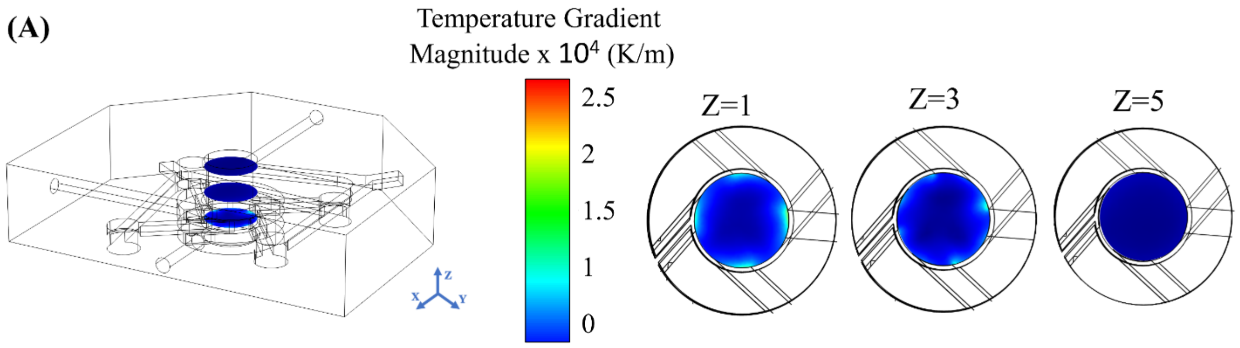

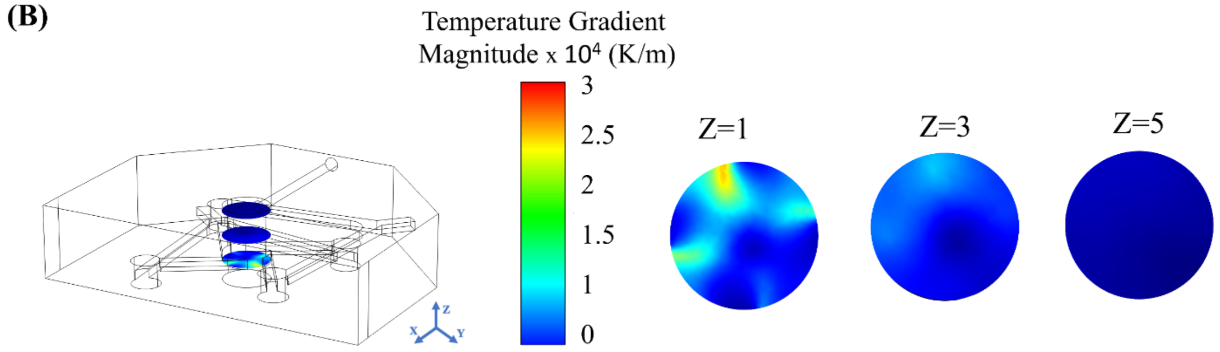

S3.6 Calculation of the Settling Velocity of α-form and β-form L-glutamic acid

The potential of the microfluidic mixer for trapping of crystals is shown by calculating the settling velocity and comparing the settling value with the[1]

$$W_s = \frac{\upsilon}{d_p}\, d^{*3}\left[38.1 + 0.93\, d^{*\left(\frac{12}{7}\right)}\right]^{-\frac{7}{8}} \quad \textbf{Eq (4)}$$

whereas υ is the fluid kinematic viscosity, d_p is the average size as $300\mu m$, and d^* is the dimensionless crystal diameter defined as:

$$d^* = \left(\frac{\Delta g}{\upsilon^2}\right)^{\frac{1}{3}} d_p \qquad \textbf{Eq (5)}$$

where $\Delta = \frac{\rho_s}{\rho} - 1$, and ρ_s and ρ are particle and fluid density, respectively, and g is the gravitational acceleration. To calculate the value for W_s the density and kinematic viscosity of water at the range of measurement. The temperature of the microfluidic mixer for all growth rate measurements is between 20 to 50°C. Table S4 includes the values of different parameters used for the calculation of the d^* and W_s.

Table S4: Parameters used for calculation of W_s of α-form and β-form L-glutamic acid

Kinematic viscosity of water at 50°C	0.5531 [$m^2.s$]
Kinematic Viscosity of water at 20°C	1.0035 [$m^2.s$]
Diameter of α-form	0.00015 [m]
Diameter of β-form	0.0003 [m]
Density of α-form	1.548 [$g.cm^{-3}$]
Density of β-form	1.603 [$g.cm^{-3}$]

The particles in the microfluidic mixer that settles down have settling velocities greater than the maximum velocity in the microfluidic mixer. The calculated W_s for both polymorphs is shown in Table S5.

Table S5: Calculated W_s value for α-form and β-form L-glutamic acid from 20 to 50 °C

20°C		50°C	
$W_{s,\text{ alpha}}$	0.54886855 [$cm.s^{-1}$]	$W_{s,\text{ alpha}}$	0.74320273 [$cm.s^{-1}$]
$W_{s,\text{ beta}}$	1.59345611 [$cm.s^{-1}$]	$W_{s,\text{ beta}}$	2.30001719 [$cm.s^{-1}$]

The maximum velocity of the microfluidic mixer is near the outlet and has a value of 0.498 [$cm.s^{-1}$], which is lower than the settling velocities shown in Table S5. Figure S6 shows the velocity streamlines in the microfluidic mixer, indicating the maximum velocity in the mixer is lower than the settling velocities shown in Table S5. Therefore, it is concluded that crystals are settled down in the mixer for the growth rate measurements.

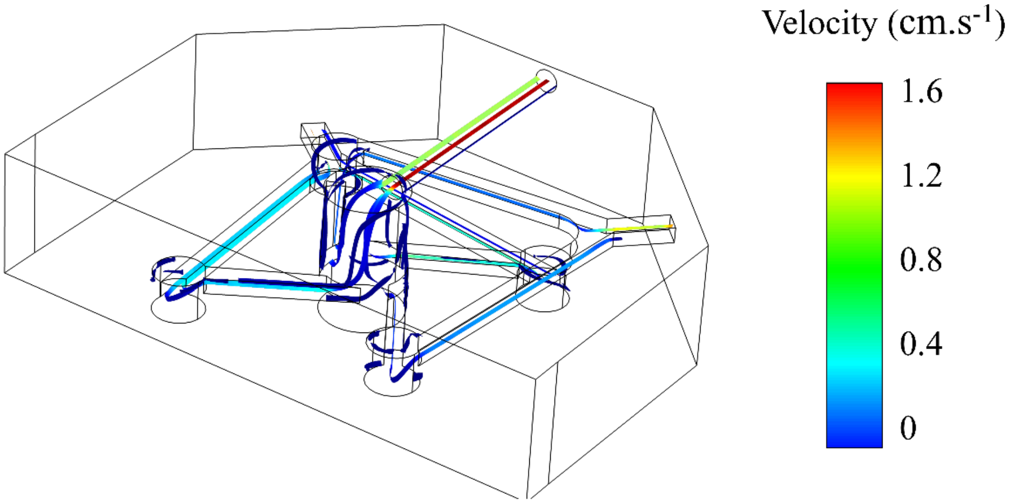

Figure S6: Velocity streamlines in the microfluidic mixer

S4. Calculation of the Residence Time Distribution

In order to calculate the residence time distribution of the merged inlet microfluidic mixer, the concentration at the outlet is recorded from $t = 0$ to $t = 15$ minutes at each flowrate. The flow rate was varied from 0.1 to 1 with increments of 0.1($\frac{ml}{min}$). Using MATLAB, these data were processed to calculate the average residence time and standard deviation at each flowrate.

The outlet concentration at different time $\bar{c}(t)$ is first divided by the initial concentration, which is set as 1 ($\frac{ml}{min}$) :

$$F(t) = \frac{\bar{c}(t)}{c_0} \qquad \boldsymbol{Eq}(\mathbf{6})$$

Here $c(0)$ is the initial concentration and $\bar{c}(t)$ is the average concentration at the outlet boundary. From here, the average residence time $\bar{t}$ and the standard deviation (σ) is calculated as:

$$\bar{t} = \int_0^\infty [1 - F(t)]dt \qquad \boldsymbol{Eq}(\mathbf{7})$$

$$\sigma^2 = 2\int_0^\infty t[1 - F(t)]dt - \bar{t}^2 \qquad \boldsymbol{Eq}(\mathbf{8})$$

The values of $\bar{t}$ and σ are calculated for each flow rate, and the results are shown in Figure S7.

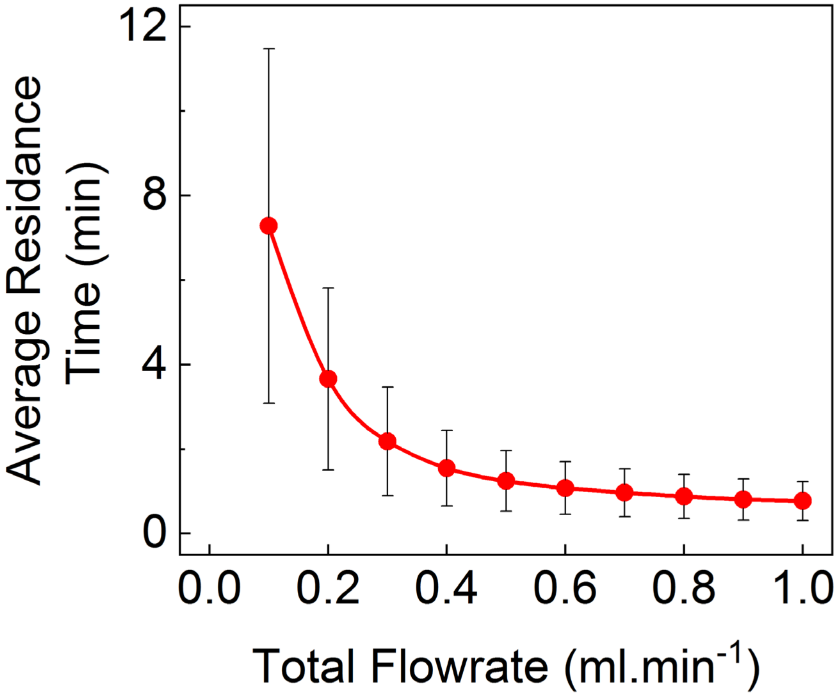

Figure S7: Average residence time distribution and variance of the micromixer as a function of flow rate.

S5. Details of Experimental Condition for Each Well in the Multi-Well

Figure S8 shows a schematic of eight cooling crystallization conditions with input temperatures for aqueous solutions of L-glutamic acid and the coolant stream. Table S6 summarizes the flow rates and concentration of L-glutamic acid in water for the initial solution, mixer, and equilibrium condition. The supersaturation is calculated as:

$$S = \frac{C_{Mixer}}{C_{equ}} \quad \boldsymbol{Eq}(\mathbf{9})$$

For samples A to H, the C_{mixer} is the concentration of the entering solution inside the micromixer, while for the mixing approach C_{mixer} is the concentration of the mixture of hot and cold streams, which is calculated as:

$$C_{mixer} = \frac{Q_{Hot}*C_{Hot}+Q_{cold}*C_{cold}}{Q_{Hot}+Q_{Cold}} \quad \mathbf{Eq}\ (\mathbf{10})$$

The C_{equ} or C^* is the concentration of the L-glutamic acid at the equilibrium temperature in the micromixer.

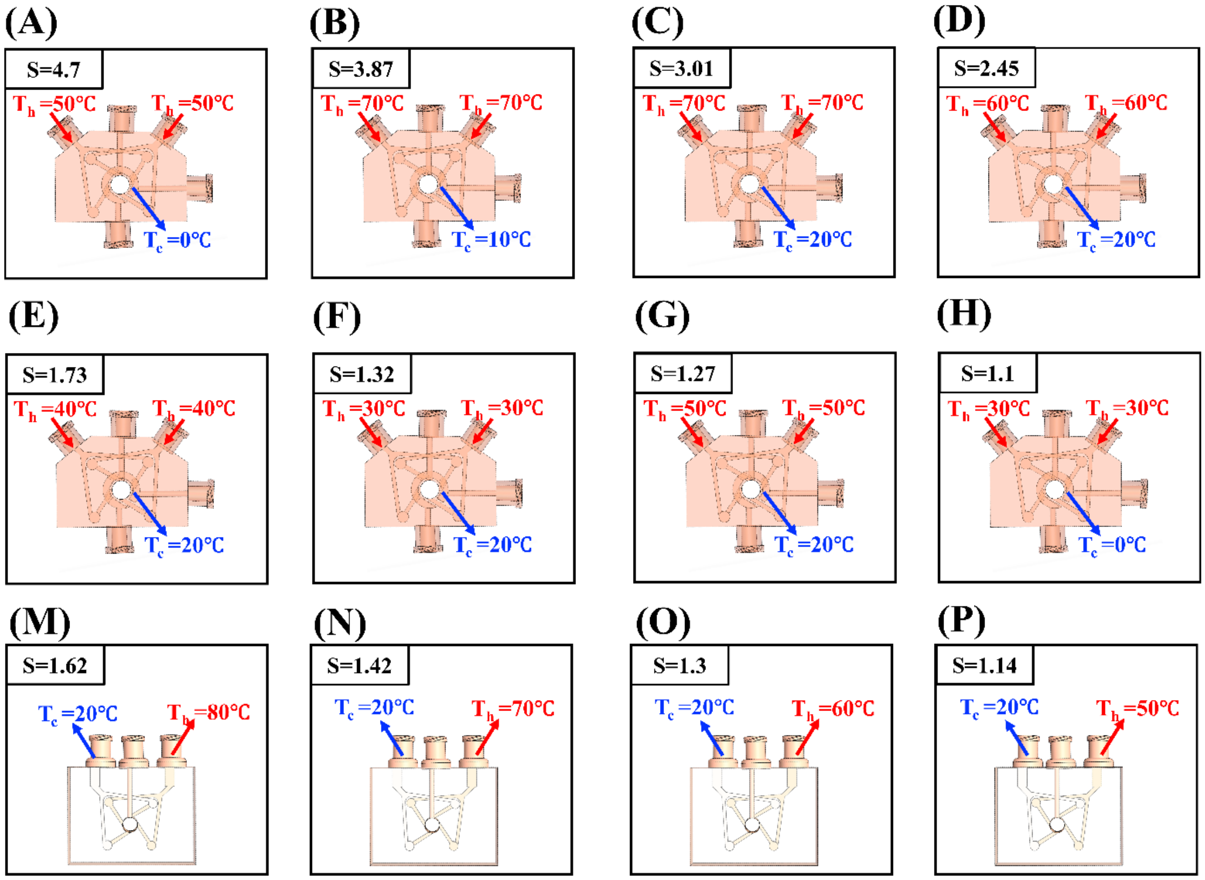

Figure S8: (A), (B), (C), (D), (E), (F), (G), and **(H)** Selected temperatures for cooling bath and saturated hot L-glutamic acid solutions in the cooling bath strategy**; (M), (N), (O),** and **(P)** Selected temperatures for saturated hot and cold L-glutamic acid solutions in the mixing hot and cold strategy.

Table S6: Details of Experimental Condition for Cooling Crystallization of the L-glutamic acid.

Samples	T_h (°C)	T_c (°C)	T_{equ} (°C)	Q_{Total} (mL.min^{-1})	$C_{Initial}$ (mol. L^{-1})	C_{Mixer} (mol. L^{-1})	C_{equ} (mol. L^{-1})	Supersaturation
A	50	0	9.30	1	0.152	0.152	0.032	4.78
B	70	10	33.19	2	0.289	0.289	0.076	3.87
C	70	20	39.37	2	0.289	0.289	0.096	3.01
D	60	20	35.39	2	0.214	0.214	0.087	2.45
E	40	20	27.59	2	0.102	0.102	0.059	1.73
F	30	20	23.77	2	0.066	0.066	0.050	1.32
G	50	20	31.46	2	0.091	0.091	0.070	1.29
H	30	0	11.27	2	0.036	0.036	0.033	1.11
M	80	20	50.00	1	0.430	0.239	0.148	1.61
N	70	20	45.00	1	0.290	0.175	0.124	1.42
O	60	20	40.00	1	0.210	0.131	0.101	1.30
P	50	20	35.00	1	0.150	0.098	0.086	1.14

S6. Comparison of the Experimental and Simulated values of the Dimensionless Variable (θ) for the Non-jacketed Micromixer

The dimensionless temperature (θ) depends on the flow rate of hot and cold solutions. In Figure S9, a comparison study between the simulated (θ) and experimentally measured is provided.

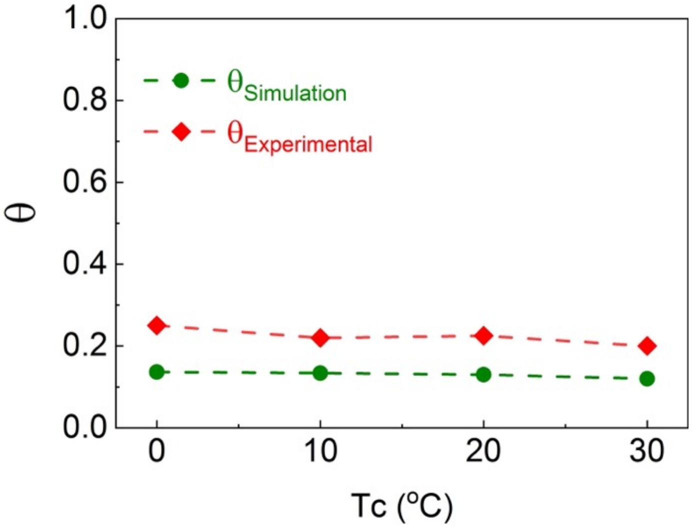

Figure S9: Comparison of the dimensionless temperature (θ) between the simulated values and the experimentally measured.

S7. Growth Rate Measurements of L-glutamic acid Polymorphs

The growth rate data were obtained by taking time-lapse images from samples every sixty seconds. The change in the distance from face 111 was divided by the time difference. Figure S10 shows a series of time-lapse images taken for sample C where the supersaturation is 3.01.

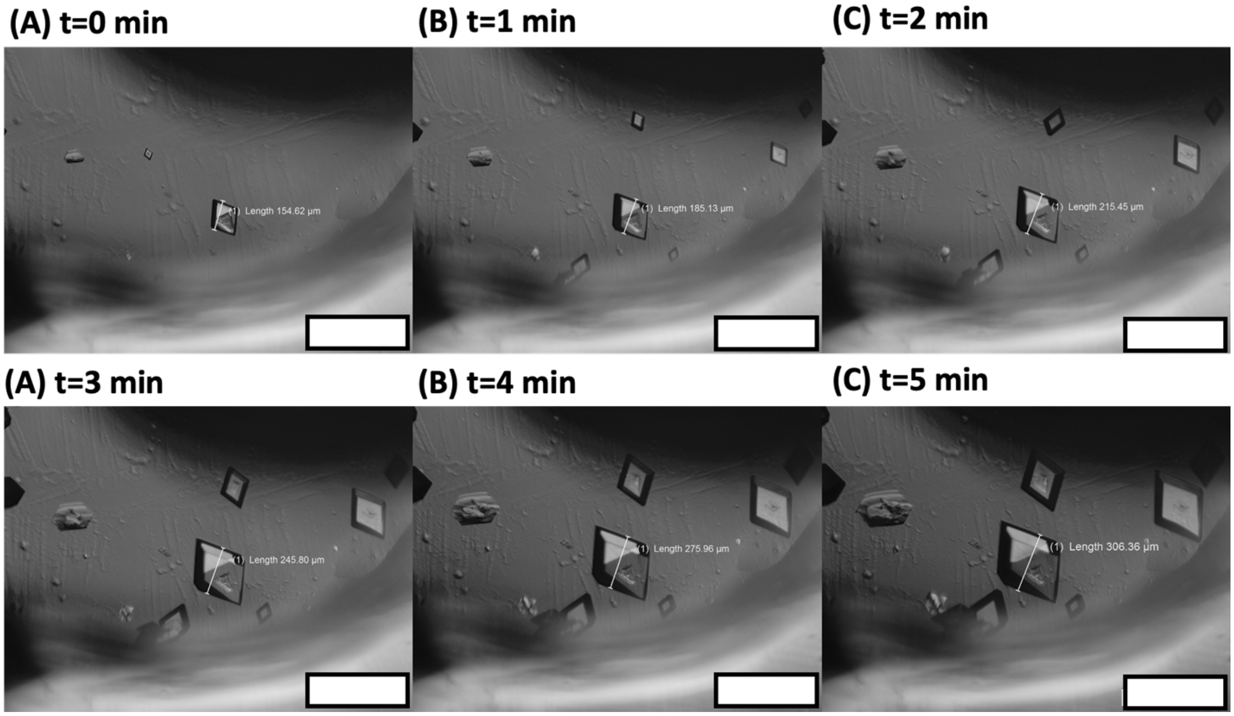
(A) t=0 min
(B) t=1 min
(C) t=2 min
(A) t=3 min
(B) t=4 min
(C) t=5 min

Figure S10: Time-lapse images from sample C (S=3.01) for 5 minutes. The $t = 0$ is not the initial time of the experiments, and it is the time when the measurements started. (The scale bar is 500 μm)

Table S7: Growth rate measurements for sample C (S=3.01)

Time(s)	Size (μm)	Growth Rate ($\mu m. s^{-1}$)
0	154.62	0.5085
60	185.13	0.5053
120	215.45	0.5058
180	245.8	0.5026
240	275.96	0.5066
300	306.36	
Mean Growth Rate ($\mu m. s^{-1}$)		0.5058
Standard Deviation (Growth Rate)		0.0019

The measured growth rates are compared with the predicted values that are calculated from equation (10):[2,3]

$$G_{B+S} = AT\, exp\left(-\frac{B}{T}\right)(S-1)^{\frac{2}{3}}\; exp\left(-\frac{C}{T^2 lnS}\right) \qquad \boldsymbol{Eq}\;(\mathbf{11})$$

$A = 3.63 \times 10 - 4\; ms^{-1}K^{-1}$;

$B = 3.72 \times 10^3\; K$;

$C = 5.42 \times 10^4 K^2$

S8. X-Ray Diffraction Patterns of L-glutamic acid Polymorphs

The XRD experiments were conducted using a Bruker D2 PHASER diffractometer with a LynxEye detector (sample to detector = 5.0 cm) and Cu-Kα source with λ = 1.54 Å (8 kV). All diffraction patterns were measured over a 2θ range of 5 to 30 with 0.02, 2θ step and a 1 s/step dwell time by which each pattern was obtained in about 21 minutes. We have reflected this information in the supporting materials section S8.

The simulated crystallography data (cif files) were obtained from the Cambridge Crystallographic Data Centre (CCDC) as follows, and the values reported for lattice unit cells from the literature are:[4-6]

- CCDC Number: LGLUAC11; Deposition Number(s): 1206531

The β-GLU crystallizes in the orthorhombic $P2_12_12_1$ space group and contains one symmetry-independent molecule (Z′ = 1), leading to a total of four molecules in the crystallographic cell (Z = 4). The unit cell has lattice dimensions of a = 5.139 Å, b = 6.879 Å, c = 17.246 Å, and V = 609.72 Å^3. [7]

- CCDC Number: LGLUAC02; Deposition Number(s): 1206529

The α-GLU crystals form in the orthorhombic $P2_12_12_1$ space group and contain one symmetry-independent glutamic acid (Z′ = 1), resulting in four zwitterionic α-GLU molecules per cell (Z = 4). The unit cell has lattice dimensions of a =7.012Å, b=8.762Å, c=10.273Å, and V=631.17Å^3.[7]

The cif files were then plotted using the crystalDiffract software that calculates diffraction patterns using the types and positions of atoms in a unit cell of a crystal. The Simulate spectra are labeled using Material Studio (V8.0.0.843) software.

Figure S11 shows simulated and experimental XRD patterns for pure α −form and β −form. The XRD of β −form was taken directly for as-purchased L-glutamic acid (Sigma-Aldrich, chemical purity≥ 99%). The pure α −form was prepared by cooling crystallization of a saturated aqueous solution of L-glutamic acid at 70°C. The experimental patterns are labeled using Material studio (V8.0.0.843) software.

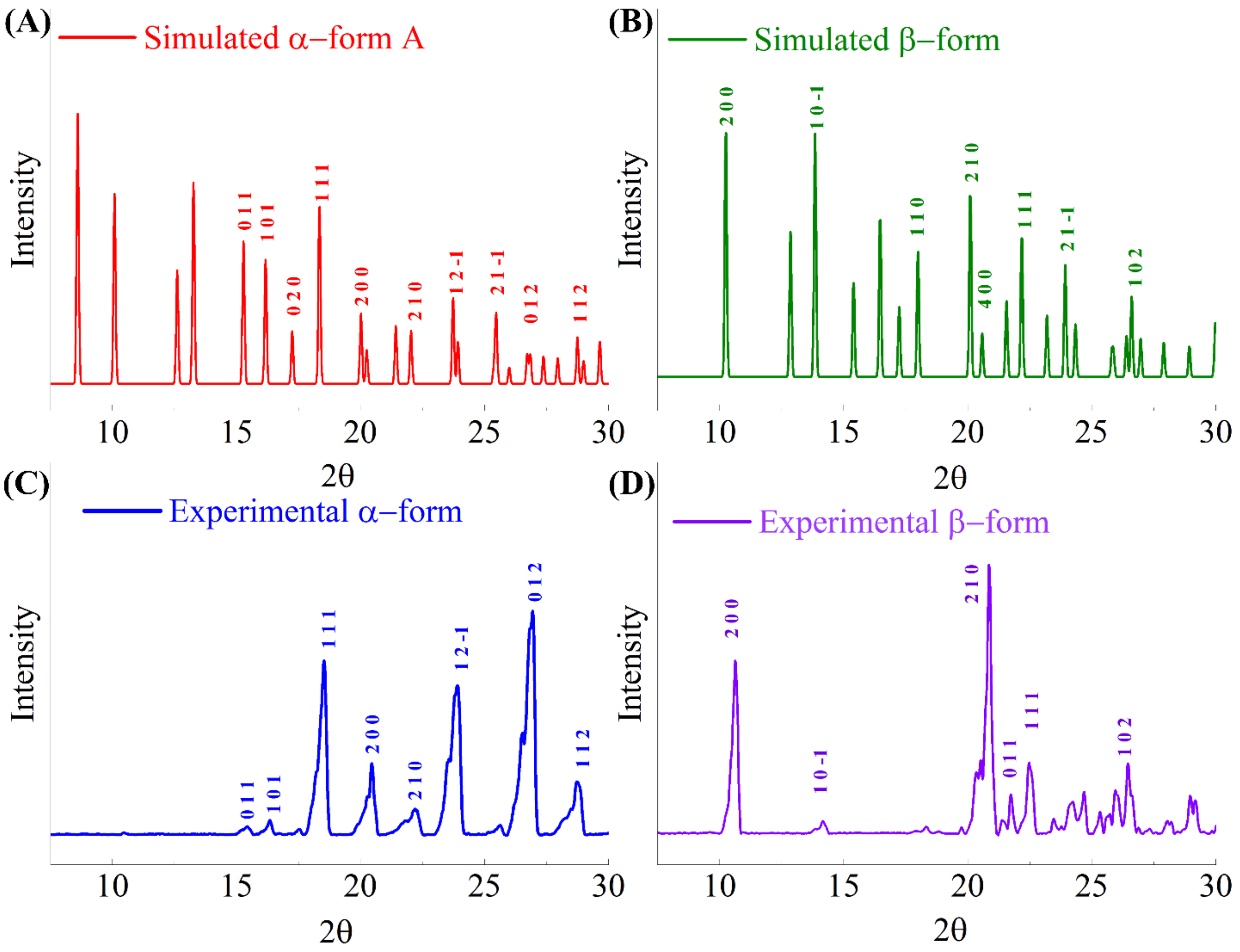

Figure S11: XRD patterns of L-glutamic acid polymorphs: **(A)** Simulated α-form, **(B)** Simulated β-form, **(C)** Experimental α-form**, (D)** Experimental β-form.

References

(1) Zhiyao, S.; Tingting, W.; Fumin, X.; Ruijie, L.: A simple formula for predicting settling velocity of sediment particles. *Water Science and Engineering* **2008**, *1*, 37-43.

(2) Schöll, J.; Lindenberg, C.; Vicum, L.; Brozio, J.; Mazzotti, M.: Precipitation of α L-glutamic acid: determination of growth kinetics. *Faraday Discussions* **2007**, *136*, 247-264.

(3) Dighe, A. V.; Singh, M. R.: Solvent fluctuations in the solvation shell determine the activation barrier for crystal growth rates. *Proceedings of the National Academy of Sciences* **2019**, *116*, 23954.

(4) Hirayama, N.; Shirahata, K.; Ohashi, Y.; Sasada, Y.: Structure of α Form of L-Glutamic Acid. α-β Transition. *Bulletin of the Chemical Society of Japan* **1980**, *53*, 30-35.

(5) Wantha, L.; Punmalee, N.; Sawaddiphol, V.; Flood, A. E.: Effect of Ethanol on Crystallization of the Polymorphs of L-Histidine. *Journal of Crystal Growth* **2018**, *490*, 65-70.

(6) Lehmann, M. S.; Koetzle, T. F.; Hamilton, W. C.: Precision neutron diffraction structure determination of protein and nucleic acid components. VIII: the crystal and molecular structure of the β-form of the amino acid l-glutamic acid. *Journal of Crystal and Molecular Structure* **1972**, *2*, 225-233.

(7) Ruggiero, M. T.; Sibik, J.; Zeitler, J. A.; Korter, T. M.: Examination of l-Glutamic Acid Polymorphs by Solid-State Density Functional Theory and Terahertz Spectroscopy. *The Journal of Physical Chemistry A* **2016**, *120*, 7490-7495.